Splashing physics of springboard diving

Long Write-Up

André Heck[1], Sebas van Baarsen[2], Jan Wilko Heinzel[2], Ad Mooldijk[3] and Norbert van Veen[3]

[1] Korteweg-de Vries Institute for Mathematics, University of Amsterdam, Amsterdam, The Netherlands
[2] Indoor Cliff Diving, Amsterdam, The Netherlands
[3] CMA-Science, Amsterdam, The Netherlands

Abstract

Understanding rotational physics can be challenging for several reasons. Firstly, rotational motion involves physics concepts such as torque, angular momentum, and moments of inertia, which are more abstract and difficult to visualise compared to linear motion. Secondly, studying rotational motion often requires a strong foundation in trigonometry and calculus. Thirdly, the abstract nature of rotational physics can make it harder for teachers to find interesting and doable activities for their students that connect to real-world experiences. In this paper we discuss how springboard diving and gymnastics can provide rich contexts for ICT-supported student explorations of rotational physics. These activities can vary in difficulty from moderate to advanced and very close to the level of biomechanical research conducted by practitioners. Suggested topics include video analysis of a compound motion, mathematical modelling of an athlete for estimation of his/her body segment inertia parameters, and in-depth motion analysis of springboard dives. These topics aim to enhance the understanding of the rotational physics underlying athletic movements. Mathematical modelling and motion analysis, in particular, are considered suitable for challenging practical investigations and research projects for upper-secondary students and beyond.

Keywords: rotational kinetics, biomechanics, video analysis, anthropometric modelling of the human body, estimation of moments of inertia and angular momentum.

1. Introduction

Performance in gymnastics, trampolining, and springboard or platform diving relies on the laws of physics to create complex movements of the human body. Tumbling and somersaulting in these sports provide rich contexts for studying rotational kinetics. Traditional textbook exercises, such as calculating the change in angular velocity due to a change in moment of inertia, have their utility but add little to a deeper conceptual understanding of rotational physics. In the following example of a common textbook exercise

> *A diver can reduce her moment of inertia by a factor of about 3.5 when changing from the straight position to the tuck position. If she makes 2.0 rotations in 1.5 s when in the tuck position, what is her angular speed (rev/s) when in the straight position?* (example taken from [1])

a student gets an answer by plugging values into the law of conservation of angular momentum. The task does not give any insight in how to compute the moment of inertia and why it is smaller in a tucked posture than in layout posture. In contrast, rich contexts for studying rotational physics, such as the giant circle on the high bar [2,3], the Jäger salto [4], and a toppling dive from a standing position on a springboard [5], could involve activities where students really use physics and mathematics concepts to understand human movements

This paper focuses on a key skill in gymnastics and diving: the somersault. Most body rotation occurs while the athlete is airborne, with postures and postural changes determining the amount of rotation achieved. For simplicity, we restrict our study to non-twisting somersaults in diving from the 3-m springboard, from take-off to water entry, carried out by two. elite cliff divers The methods used apply equally well to similar movements in gymnastics, so we use the term “athlete” instead of “diver”, unless discussing a diving-specific topic.

Basic measurement tools like a folding rule and a flexible tape measure turn out to be sufficient for obtaining accurate values of lengths and circumferences of body segments required to estimate inertia properties. Using video analysis and modelling tools in the COACH environment [6,7], and using principles of physics, we analyse several dive types. The goal

is to scientifically understand the rotational difficulty level of differing somersault types and how athletes adapt their techniques to achieve the intended amount of rotation.

The paper is organised as follows. The second section is an introduction to springboard diving and commonly used vocabulary in the sport and science of diving. In the third section we carry out a video analysis of a forward three-and-a-half somersault in a tucked posture, in which we describe the compound movement of the human body in terms of a linear and rotational component. The fourth section is about the development of a suitable mathematical model of the human body for motion analysis. We aim to find an anthropometric model composed of rigid body segments to estimate inertia properties of individual athletes and compute moments of inertia for three common postures: layout, pike, and tuck. We apply this model to our two athletes and compare the results with biomechanic research outcomes. The fifth section is a thorough motion analysis of an athlete while airborne in a forward three-and-a-halve somersault in a piked posture, using the mathematical model of the human body to compute changes in moments of inertia and verify the constancy of angular momentum. In the sixth section we carry out a similar motion analysis for a forward two-and-a-halve somersault in a piked posture. The final section is a discussion of how the scientific explorations of diving presented can serve as examples of authentic practical investigations and research projects for upper-secondary students and beyond, enabling them to act as sport scientists using principles of physics and mathematical methods to understand complex human movements.

2. Bird's eye view of springboard diving and biomechanical research

This section provides a brief overview of springboard diving and related biomechanical research. We

1. describe the different phases of a dive;
2. explain the naming conventions for competitive dives;
3. discuss the orientation of the athlete's body during a dive;
4. outline the biomechanical principles that help understand the athlete's movements during the flight phase.

2.1 Phases of a springboard dive

A dive consists of the starting position, approach, take-off from the board, flight, and entry into the water. In competitive diving, the primary goals are to generate sufficient angular momentum to execute an announced number of somersaults and twists, obtain height for extended air time to perform acrobatic manoeuvres, and travel safely but not excessively away from the board, as this affects the diving score awarded by judges [8]. These objectives are mainly determined at the end of the take-off. Once airborne, the athlete can only control the speed of somersault rotation by altering body shape and must appear graceful while performing acrobatic manoeuvres. The dive should finish with the body straightened and arms extended overhead to minimise splash upon water entry.

In non-armstand dives, the athlete must start in a straight, upright position with the head aligned with the body, elbows straight, and feet together. In armstand dives, the athlete must achieve an inverted, vertical position with straight elbows, feet together, toes pointed, and show steady balance before take-off [9]. There are six groups of dives, of which the first four are determined by the direction the diver rotates: forward, backward, reverse, inward. In addition, there is the twisting group of dives that use a twist and the armstand group of dives in which the divet assumes a handstand position on the edge of the platform before the dive start. The approach varies by dive group. In the backward and inward groups, the athlete starts at the end of the board, activates board movement, and then executes the final push. In the forward and reverse groups, a running approach is used to gain height. The athlete starts near the back of the board and walks forward, finishing with a jump (called a hurdle) to land on the end of the board ready for take-off. At the end of hurdle flight, the diver contacts the board using two feet to depress it, storing elastic energy for the take-off. Greater hurdle height results in more energy to depress the board, aiding in a higher jump. Angular momentum needed to initiate rotation is generated during the recoil phase through hip flexion in forward dives, which must be achieved before leaving the board as angular momentum is conserved once airborne. This is a conceptual understanding of rotational dynamics that students need to come to grips with before they can explore somersaults in greater depth.

The approach and take-off phases are intriguing topics for student investigations, including studying the oscillations of the springboard during and after take-off; the interested reader is referred to [10-14]. However, this paper focuses on the airborne phase, from take-off to water entry. Neglecting air friction, the athlete's angular momentum remains constant in magnitude and direction once airborne, with angular velocity changes limited by the postures that the athlete can physically move between or hold.

2.2 Dive number

A dive number is an alphanumeric code that describes precisely the dive that is (to be) performed. For example, 107C indicates a forward (1) somersault (0) with three-and-a-halve rotations (7) in a tucked posture (C). The code always begins with three or four numerals, follows by a letter.

The first digit in a dive number indicates the group to which the dive belongs: 1 for forward, 2 for backward, 3 for reverse, 4 for inward, 5 for twisting, and 6 for armstand.

The second digit for the first four dive groups (forward, backward, reverse, inward) is 0 for a somersault and 1 for a flying somersault, which is a dive in which the athlete assumes a straight position from take-off, or after one somersault in a dive, before executing the remainder of the dive.

The third digit describes the number of half somersaults: 1 for $\frac{1}{2}$ somersault (a dive), 2 for 1 somersault, 3 for $1\frac{1}{2}$ somersaults, and so on. The fourth digit is only used in twisting somersaults and describes the number of half twists.

Finally the letter denotes the main body posture during flight: A for layout, B for piked, C for tucked, D for free position. The layout, piked, and tucked postures are defined by the angles of the hip and knee joints (see, for instance, [15]).

Figure 1 shows artist impressions of diving figures discussed in this paper, illustrating differences between backward and forward diving, and between a layout, piked and tucked posture during a dive. They are not realistic paintings of dives: the posture of a diver at take-off is not the same for all diving figures and a vertical entry as shown is not possible in reality.

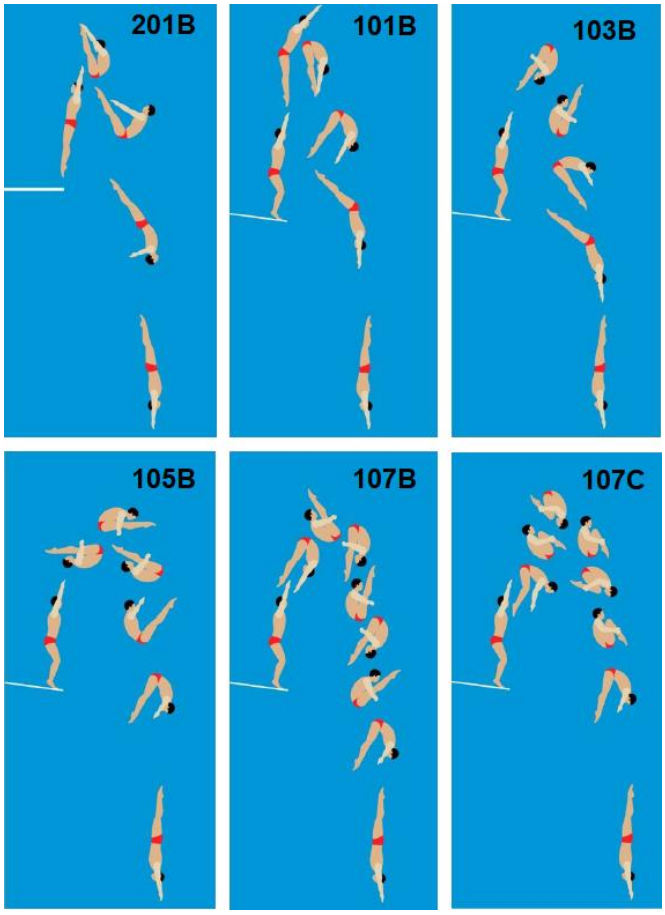

Figure 1. Artist impressions of diving figures (after [9]). In the 201B dive, for example, the athlete changes posture from layout to pike, and back to layout. In the 107C dive, the athlete changes posture from layout to tuck, and back to layout.

Figure 2 overlays images from video recordings of a 107C and a 103B dive, showing the athlete leaning forward at take-off to generate rotation. The conservation of angular momentum prevents the athlete from stopping rotation mid-air, thus underwater movements are used to create the illusion of a vertical entry for the judges.

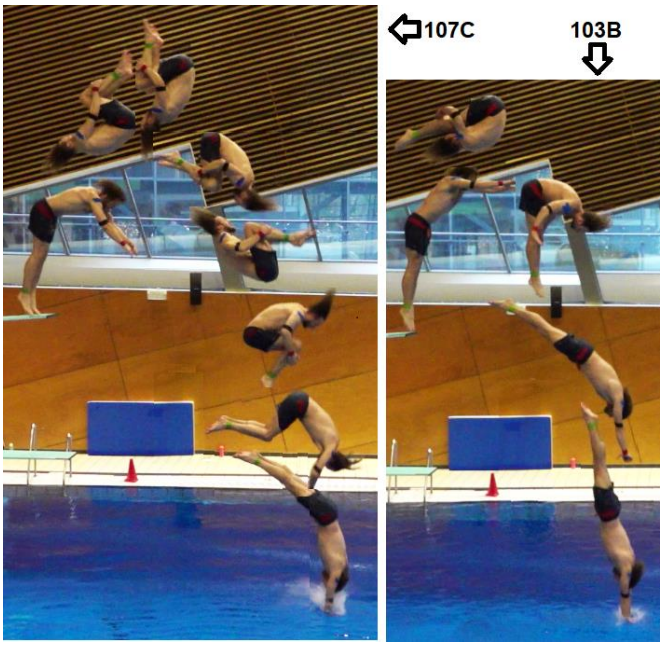

Figure 2. Overlays of images of postures during a video recorded dive with dive number 107C (left) and 103B (right).

2.3 Body orientation angle

A somersault involves the rotation of the human body about a horizontal axis that is parallel to the ground and perpendicular to the direction of travel. In a pure rotation, this axis aligns with the transverse axis of the body. To describe rotational motion, we use a moving non-rotating 3D reference frame centred at the athlete's centre of gravity with a standard biomechanical choice of orientation of axes. The positive z axis is upward relative to the springboard at rest. The y-axis is the horizontal axis about which the somersault occurs. In a pure forward somersault it is parallel to the transverse axis and directed from left to right. The x-axis aligns with the direction of travel for forward and backward somersaults.

If the athlete maintains a fixed posture during flight, the body can be treated as a single unit, and a specific point or body segment can be used to describe the rotation. In section 3 we use this approach to describe the rotation of an athlete in a tucked posture during a 107C dive. However, when the athlete changes the posture during flight, defining its orientation relative to the reference frame becomes less obvious. For instance, figure 3 illustrates the postures of an athlete performing a 201B dive, transitioning from a layout position at take-off to the next layout posture after piking.

After take-off, the overall rotation of the body must be in the clockwise direction at a low angular speed. Using the hip as the origin of the moving non-rotating reference frame, the torso initially moves counter-clockwise, opposite to the whole body's rotation. This counter-clockwise movement is compensated by the fast clockwise movement of the lower extremities.

Consequently, neither the torso nor the lower extremities are suitable for describing the rotation of the whole body.

Figure 3. A series of stills from a video recording of a 201B dive, from layout to layout posture via an intermediate piked posture. The time lapse between consecutive stills is 2/15 s.

Yeadon [16] proposed using the orientation of the line from the midpoint of the knee to the midpoint of the shoulder, as this choice is less sensitive to changes in the hip angle than using a single body segment. The angle between the vertical axis and this line is called the body orientation angle. Figure 4 shows the time course of the body orientation angle obtained by video analysis of a 201B dive (blue graph). The graph indicates a nearly constant rotation at a low angular velocity of 124°/s (the slope of the linear fit in black). The other graphs show the orientation angles based on the lines through the hip and torso (orange graph) and the lower extremities (red graph). These angles are less suitable for describing whole-body rotation. The torso orientation angle and the body orientation angle converge as the athlete straightens his body and prepares for entry into the water, though not as perfectly straight as in artistic impressions.in figure 2. Images of postures below the diagram show the body orientation line and angle at several moments: take-off ($t = 0$), mid-flight ($t = 0.2, 0.5, 0.8, 1.1$), and water entry ($t = 1.33$s).

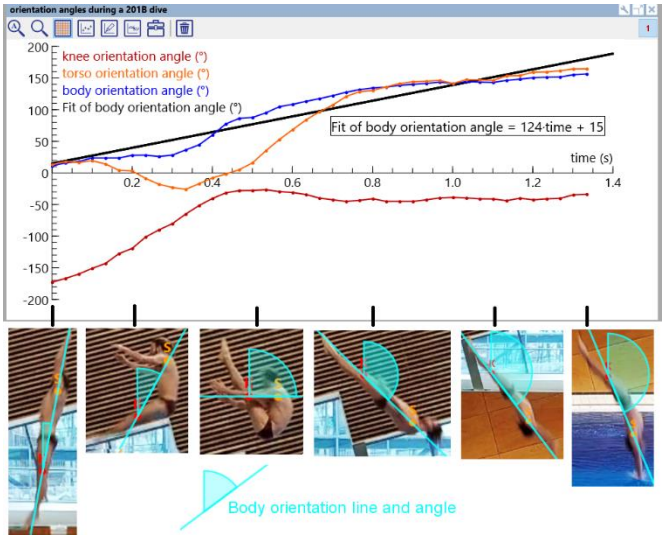

Figure 4. Time course of three orientation angles during a 201B dive.

We propose using the orientation of the line from the centre of gravity of the lower extremity to the centre of gravity of the torso. In this way we avoid a measurement of the position of the knee in case of a piked dive. We call the angle between the vertical axis and this line the somersault angle.

Discussing the definition of orientation of the human body during somersaults in a classroom setting can be highly beneficial. Students often do not realise that definitions in physics can be ambiguous when applied to real-world contexts. In the context of diving, one could also discuss various interpretations of dive height and flight time. Once these definitions are agreed upon, students can explore how these quantities, as well as body segment angles, change during a dive. They can also compare experimental data from different diving figures and amongst various athletes. This type of investigation closely resembles the research work done by sports scientists.

2.4 Biomechanical principles for understanding somersaults

Understanding somersaults requires grasping key principles of rotational dynamics, including angular velocity and acceleration, torque, angular momentum, moment of inertia, rotational kinetic energy, and centripetal and centrifugal force. These concepts are challenging for students [17-20], who often hold alternative conceptions such as:

- Any force acting on an object produces a torque;
- Torque is the same as force and has the same direction;
- Constant torque leads to constant angular velocity;
- An object moving with constant velocity in a straight line has zero angular momentum;
- Angular momentum is not a vector;
- The direction of angular momentum is in the direction of linear momentum;
- Angular momentum is an intrinsic property that does not depend on the reference frame;
- Linear and angular momentum are conserved jointly, with one converting into the other (similar to energy conversion from one form into another).

Somersaults involve a complex combination of planar motion (about a point mass) and the rotation of a non-rigid body composed of rigid body segments. To understand this, one usually learns rotational kinetics starting from a point-like object, progressing to a system of point-like objects, and via a rigid body finishing with a system of rigid bodies that can change positions relative to each other. We do not discuss here such learning trajectory, but only remark that reports recommend video analysis projects [3, 21-23] or laboratory experiments with sensors [24] for helping students better grasp the physics of rotational motion.

What simplifies the exploration of somersaults is the restriction to pure somersaults, i.e. to planar motions of the human body that involve only rotation about an axis perpendicular to the plane of motion. This allows the motion to be described by linear kinetics of the centre of gravity and angular kinetics about the axis through the centre of gravity. The angular momentum vector in this case aligns with the rotation

axis, making it easier to determine its direction and focus on its magnitude.

2.4.1 Centre of gravity

Students need to understand the concept of the centre of gravity, which is the point where the body's mass is concentrated and through which gravity acts. This point may lie outside the body and depends on the arrangement and relative masses of body segments. Determination of the centre of gravity involves using a segment model of the human body, such as a five-segment model consisting of two upper extremities, two lower extremities, and one segment for the head-neck-torso (see figure 5), or a more complicated model such as the fifteen-segment model of Hanavan [25], discussed in section 4. In all cases, one uses the mass and centre of gravity of each body segment to determine the centre of gravity of the whole body. Mass and location of the centre of gravity of each segment can be estimated by the use of anthropometric tables published in papers or biomechanics textbooks (e.g. [26-31]).

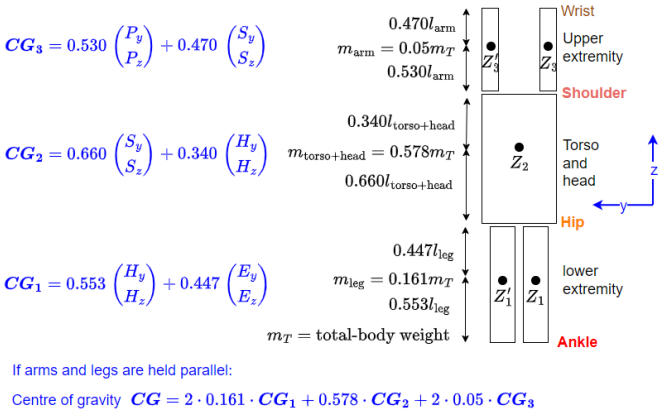

Figure 5. Sample calculation of the location of the centre of gravity for a five-segment model of the human body.

Note that the definition of the centre of gravity (CG) of the human body modelled as a system of body segments connected by frictionless rotary joints implies that the sum of the segmental torques about CG due to gravity must be equal to zero. For an airborne athlete, the net torque about the axis of rotation through CG must therefore be zero (unless other forces such as air friction intervene) and the angular momentum cannot change during the flight phase. The vector $\overrightarrow{r_{\text{CG}}}$ from the origin of the frame of reference to CG can be computed from the known segment masses m_s and the known segment vector $\vec{r_s}$ from the origin to the centre of gravity of the segment for all body segments by

$$m_{\text{tot}} \cdot \overrightarrow{r_{\text{CG}}} = \sum_s m_s \cdot \vec{r_s}$$

where $m_{\text{tot}} = \sum_s m_s$ is the total body mass. The segment vectors $\vec{r_s}$ are determined from the positions of the endpoints of the segments and their tabulated distances to the centre of gravity as fractions of the segment lengths listed in anthropometric tables. Textbooks [26-31] provide detailed information and examples for these calculations. Figure 5 illustrates the calculation for a human body modelled by five segments (the choice of the z-axis is adopted from mathematical modelling of the human body in section 4).

2.4.2 Moment of inertia and angular momentum

To understand the rotational dynamics of a somersaulting human body, we can use the body orientation angle as an approximation of the angle of rotation. The angular velocity ω of a rotating body is defined as the rate of change of this angle with its direction perpendicular to the rotating orientation line and parallel to the rotation axis. The angular momentum L (or its magnitude) of the human body, considered as a single non-rigid body, rotating about an axis through the centre of gravity can be expressed as $L = I \cdot \omega$, where I is the moment of inertia of the human body about the axis of rotation. The moment of inertia I and the angular velocity ω are not constant during a somersault due to postural changes, but their product remains constant. The moment of inertia for any posture can be computed by summing the moments of inertia for all body segments about the axis of rotation. Section 4 will detail how these moments of inertia can be estimated using the geometrical modelling and the parallel axis theorem to compute segmental moments of inertia about their centres of gravity.

A precise, albeit more complex, method to compute the angular momentum L of a rotating human body, which does not rely on an ambiguous angle of rotation or treat the body as a single non-rigid object, involves the following (cf. [26, 31]): The angular momentum L_s of each segment s about the transverse axis through the human body's centre of gravity CG can be computed as the sum of a local and remote term:

$$L_s = I_s \cdot \omega_s + m_S \cdot {d_s}^2 \cdot \omega_g$$

In the first term, called the local term, I_s is the segment moment of inertia and ω_s is the segment angular velocity, both with respect to a transverse axis through the centre of gravity of the segment. In the second term, called the remote term, m_S is the segment mass, d_s is the distance between the centre of gravity of the segment and CG, and ω_g is the angular velocity of the centre of gravity of the segment about the transverse axis through CG. If ω_s and ω_g are equal (denoted by ω), this simplifies to $L_s = (I_s + m_S \cdot {d_s}^2) \cdot \omega$. According to the parallel axis theorem, this can be expressed as $L_s = I(s) \cdot \omega$, where $I(s)$ is the moment of inertia of the segment s about the axis of rotation through the body's centre of gravity. So we are back to the formula where ω is the rate of change of the body orientation angle, but one must keep in mind that it is valid only when the athlete maintains a fixed posture in an airborne somersault.

The remote term can also be expressed in terms of the third component of the cross product of the position vector $\vec{r_s} = (r_{sx}, r_{sz}, 0)$ in the plane of motion, which goes from CG to the centre of gravity of the segment, and the linear velocity vector $\vec{v_s} = (v_{sx}, v_{sz}, 0)$ of the centre of gravity of the segment:

$$[\vec{r_s} \times \vec{v_s}]_3 = r_{sx} \cdot v_{sz} - r_{sz} \cdot v_{sx}$$

The total body angular momentum L can be computed as:

$$L = \sum_s I_s \cdot \omega_s + \sum_s m_s \cdot [\vec{r_s} \times \vec{v_s}]_3$$

This formula is advantageous because the required vectors in the second sum can easily be determined using video analysis and data analysis tools, like the ones in COACH [6,7].

The moment of inertia I_s of the segment s about the transverse axis through the centre of gravity of the segment, is usually expressed as

$$I_s = m_s \cdot {k_s}^2 = m_s \cdot (\rho_s \cdot l_s)^2$$

where m_S is the segment mass and k_s is the radius of gyration, which is often expressed as a proportion ρ_s of the segment's length l_s. General estimates of radii of gyrations of human body segments are available in many biomechanics textbooks [26-31], and for our explorations, we use Table 4.1 in [29] to compare results with outcomes reported in research literature.

3. Putting a twist on a 107C dive

To better understand the biomechanics of a 107C dive, we start with a video analysis activity that is accessible and insightful for students. The dive number 107C refers to a forward $3\frac{1}{2}$ somersault in a tucked posture. Figure 6 shows a screenshot from a video analysis of this dive from a 3-m springboard. In the upper-left window, a still image captures the athlete exiting a tucked posture and preparing for water entry. The open yellow points indicate locations of the athlete's head, marked by point-clicking in the selected frames. The closed orange dots trace the trajectory of the centre of gravity (CG), estimated through mathematical analysis of the head's motion while the athlete is in a tucked posture.

The analysis is based on the assumption that the motion can be decomposed into a parabolic trajectory, approximating the CG's motion under gravity, and a sinusoidal trajectory, describing the rotational motion of the body in a tucked posture. The computational engine for this analysis is the least squares regression method of peeling-off functions [32]. The lower-left window in figure 6 displays the time course of the vertical position data with a quadratic function fit representing the head's motion trend. Next, the residual is fitted to a sinusoid by subtracting the quadratic fit from the data and determining a sinusoidal regression curve. The lower-right diagram shows this result. The sum of the quadratic and sinusoidal fits accurately describes the vertical position of the diver's head, as seen in the corresponding curve in the upper-right window.

A similar analysis for the horizontal motion of the head reveals a linear trend function. Both analyses yield an angular frequency of $15.67 s^{-1}$, corresponding to an angular velocity of $898°/s$ ($\approx 2\frac{1}{2}$ rotations per second). The linear and quadratic trend functions of the head's horizontal and vertical position, respectively, can serve as coordinate functions of an imaginary point and displayed as overlay in the video clip. The trajectory of this imaginary point (shown as closed orange dots in the video window) suggests that it is close to the athlete's hip, indicating that CG in a tucked posture is near the hip.

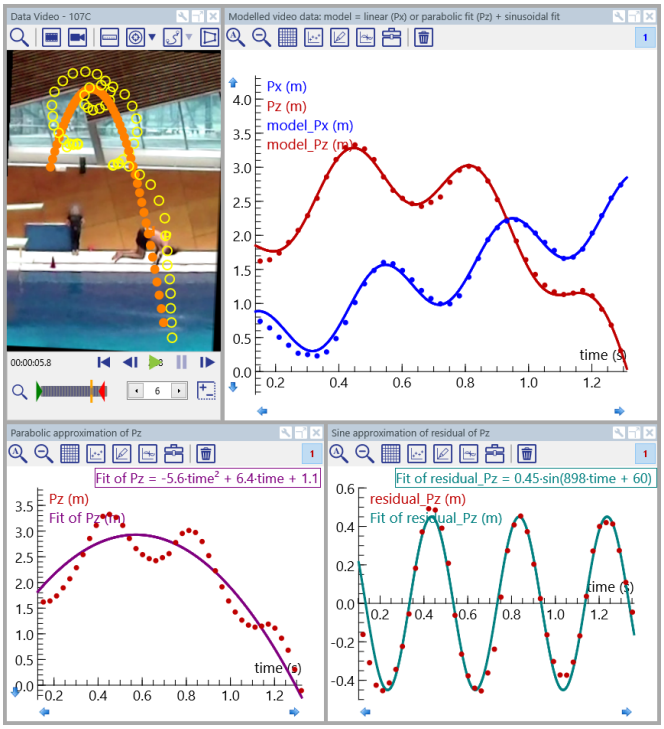

Figure 6. Video analysis of a 107C dive as compound motion. The lower windows show a parabolic fit of the vertical position of the athlete's head and a sinusoidal fit of its residual. The sum of these fits model the vertical position the head, graph of which is shown in the upper-right window, together with the model curve for the horizontal position of the head.

The above result of the video analysis opens the opportunity for students to analyse the forward $3\frac{1}{2}$ somersault in a tucked posture using a different method. They can employ a moving coordinate system with its origin always at the athlete's hip and measure the shoulder's position in polar coordinates. In essence, they use the hip-to-shoulder segment as the line of body orientation and determine the somersault angle, defined as the angle between the vertical axis and the line of body orientation.

The upper-left window of figure 7 displays a still from the video clip where the athlete is in a tucked posture; the video clip is the same as in the previous video analysis. The moving coordinate system is centred at the hip, and the shoulder centre is marked as the point of interest. By using the polar coordinates of this point, students can generate a continuous time course of the somersault angle. This time course, shown in the upper-right window, includes a linear fit for the duration when the athlete is in a tucked posture. The slope of this linear fit estimates the angular velocity, which is found to be $907°/s$, slightly higher than the value obtained using the first method.

The angular velocity of the athlete performing the airborne somersault in a tucked posture is the derivative of the somersault angle and can also be computed numerically. Ideally, students find that the angular velocity remains constant while the athlete holds the tucked posture and decreases as the athlete opens up to prepare for entry into the water. The lower window in figure 7 shows the graph of the angular velocity obtained using an advanced numerical differentiation algorithm: a generalised cross-validatory penalised quintic spline-smoothing based algorithm [33], available in the COACH environment [6,7]. A horizontal line that best fits the period when the athlete is in a tucked posture is added, showing an angular velocity close to the values found before.

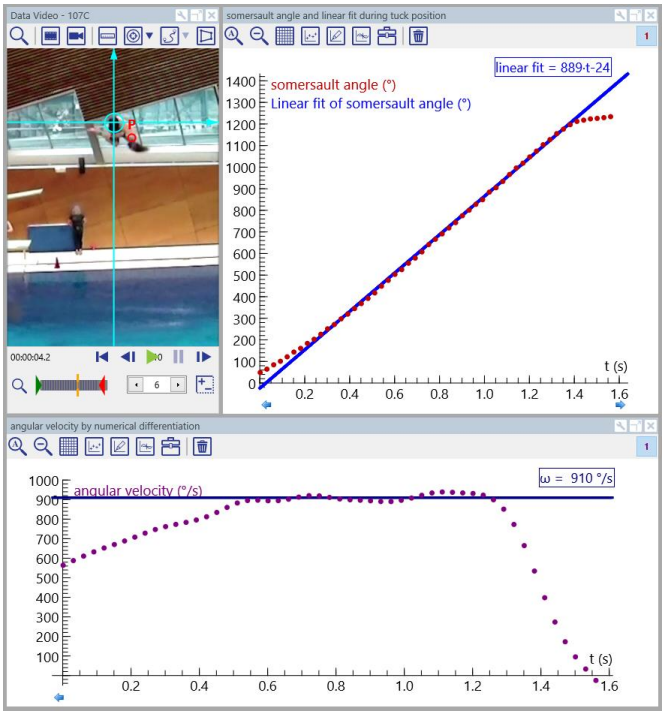

Figure 7. Video analysis of the somersault angle in a 107C dive, using the hip-shoulder segment as line of orientation.

The graph in the lower window of figure 7 connected with events in the video clip indicate that a change of posture causes a change of angular velocity. This may lead to an alternative conception that a change of posture causes a rotation of the human body. Students would not be the first to think so: It was once believed that take-offs for all dives were the same, like in figure 1, and that rotation was only generated during flight by arms and head movement. For example, Billingsley [34] wrote about the forward tuck dive: "Rotation is generated by moving the arms and head towards the knees. (p.11)." Another misconception is that a net torque is required to initiate body rotation. Frohlich [35] demonstrated that limited body rotation can be achieved without torque and used a physics-based simulation to create a series of postures leading to a torque-free back quarter somersault. Edwards [36] provided simple explanations for zero angular momentum turns, including somersaults. Essén and Nordmark [39] showed that 180° rotation can be achieved by purely internal torques and forces, keeping total angular momentum zero.

For dives, a net torque is needed to initiate rotation and this is, as we mentioned earlier, created during take-off. Figure 8 illustrates the horizontal and vertical forces acting on a stick model of the athlete at the moment when he leaves the springboard, providing the torques to initiate rotation for a 107C dive. An estimated centre of gravity (CG) is also shown.

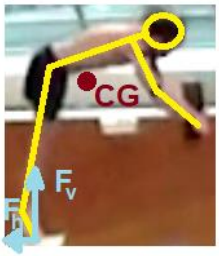

Figure 8. A stick model of the athlete at take-off, the position of the centre of gravity (CG), and the horizontal and vertical forces ($\overrightarrow{F_h}$ and $\overrightarrow{F_v}$) providing the torques to initiate forward.

What figure 8 does not show is that the athlete near the end of the recoil phase of take-off bends the hips and rapidly throws his arms forward. Rotating the body and arms in the forward direction generates angular moment and the faster this rotational movement, the larger the angular momentum. If the body were free in space, the lower part of the body would rotate in the opposite direction due to conservation of the angular momentum. However, as the athlete's feet remain in contact with the springboard, the board exerts a horizontal force on the athlete that resist this opposite direction. This horizontal force $\overrightarrow{F_h}$ provides a torque on the athlete, contributing to the somersault's initiation. The vertical reaction force $\overrightarrow{F_v}$ of the springboard also produces a torque on the athlete when he is leaning forward, with the centre of gravity not passing through the line of reaction force.

We believe that a qualitive analysis of somersaulting as in the previous paragraph is as important as quantitative analysis of biomechanical variables. Qualitative analysis, described by Knudson [38] as "systematic observation and introspective judgment of the quality of human movement for the purpose of providing the most appropriate intervention to improve performance," helps students realise that qualitative biomechanical concepts are essential for understanding body movements. Quantitative analysis can substantiate or question qualitative outcomes, or provide more details, but it does not alone enhance conceptual understanding of mechanical laws. In sections 5 and 6, we carry out detailed video analyses of a 107B dive (a forward $3\frac{1}{2}$ somersault in a piked posture) and a 105B dive (a forward $2\frac{1}{2}$ somersault in a piked posture) with the intention to verify numerically the law of conservation of angular momentum. We also estimate and compare kinematic variables for these two dives.

4. Anthropometric modelling of the human body

The following assumptions are commonly made in the design of a mathematical model of the human body:

- The human body can be represented by a set of rigid bodies of simple geometric shape and uniform density, called segments, which each closely approximate the size, shape, mass, and centre of mass of the segment;
- Regression equations for segment weights from research literature [39,40] are valid for participants in a biomechanical study;
- Limbs move about fixed pivot points when the body moves. They are often the base of the neck, the arm-shoulder, the elbow joints, the wrist joints, the leg-pelvis sockets, the knee joints, and the ankle joints.

Under these assumptions, Hanavan [25] designed a fifteen-segment geometrical model shown in figure 9, on the left-hand side. For later use, we have indicated the orientation of the coordinate system used to estimate inertial properties of segments and the geometrical shapes involved in this estimation. Twenty-five anthropometric dimension are needed to calculate properties of the model, including geometric measures like volume, area, centre of gravity, and inertia tensors. These measurements involve the total-body weight, several body heights, lengths and circumferences of limbs, and depths and breadths of parts of the torso.

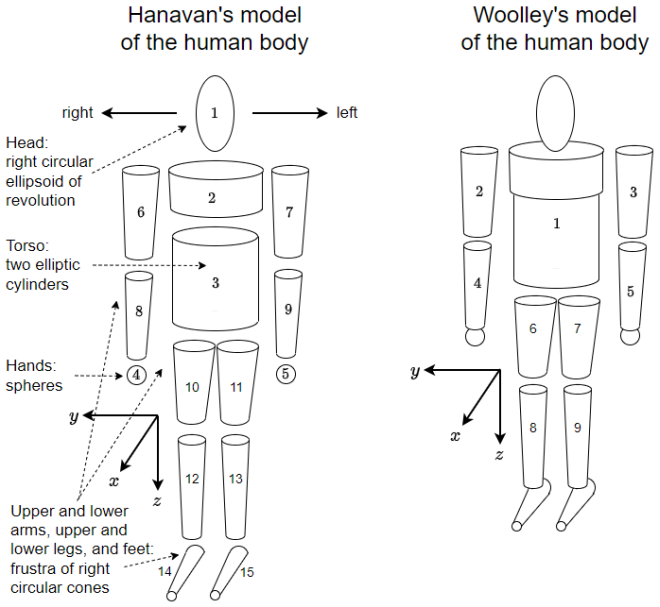

Figure 9. Hanavan's model of the human body and Woolley's simplification (after [41]).

Hanavan's model is the first in a series of more detailed geometric models [16, 41-44]. They vary in the number of segments and geometrical shapes, particularly in modelling the torso [44]. Woolley [41] simplified Hanavan's model to a nine-segment model by combining the head, neck and torso into one segment, and each lower arm with the hands. This simplified model is shown on the right-hand side of figure 9.

We use the same numbering of body segments as Hanavan [25] and Woolley [41] for a model of the human body based on the downward direction in a standing position,although other more biomechanics-driven numberings are possible. For instance, Huston [45] numbers segments in ascending progression away from the lower torso segment (numbered 1), defining the proximal and distal endpoints of the segments: The point nearer to the lower torso is the proximal endpoint, and the point further away is the distal endpoint. Thus, the shoulder (elbow) is the proximal (distal) endpoint of the upper arm, the knee (ankle) is the proximal (distal) endpoint of the lower leg, and so on.

4.1 Mass distribution

The total body mass of an individual is distributed across each body segment using regression equations. Popular choices for these equations include those by Barter [39] and Clauser et al [40]. In a study of 30 highly skilled adult male athletes from various sports disciplines, Miller and Morrison [46] did not establish the definitive superiority of Clauser et al.'s equations over Barter's equations. Clauser et al's approach requires measurements of body fat, which involve tools that are not easily accessible to students. Therefore, we use the Barter's regression equations, as Hanavan [25] and Woolley [41] did. We follow Woolley's approach, where the mass input into the regression equations is adjusted so that the sum of the regression equations equals the total body mass:

mass of head, neck, trunk = $HNT = 0.47m'_T + 5.44$ kg
mass of both upper arms = $BUA = 0.08m'_T - 1.32$ kg
mass of both forearms = $BFO = 0.04m'_T - 0.23$ kg
mass of both hands = $BH = 0.01m'_T + 0.32$ kg
mass of both upper legs = $BUL = 0.18m'_T + 1.45$ kg
mass of both lower legs = $BLL = 0.11m'_T - 0.86$ kg
mass of both feet = $BF = 0.02m'_T + 0.68$ kg

where

$$m'_T = \frac{m_T - 5.48}{0.91}.$$

The corrected total mass of the modelled man m'_T distributes the total body mass m_T proportionately to the segment masses.

Table 1 lists the predicted segment weights (kg) for the two athletes involved in our biomechanical study, indicated in slanted font. These weights are also presented as percentages of total body weight. These percentages align well with the results of Miller and Morrison [46].

4.2 Segments' centres of mass and moments of inertia

For computations of the centres of mass, moments of inertia for the body segments, and the total body of individual athletes we use the stick model of Woolley's model of the human body [44] shown in figure 10. It also shows that we use joints as endpoints of the body segments.

Body part	*Athlete 1*	*Athlete 2*	*Miller & Morrison*	
			mean	*std. dev.*
Head	*6.12*	*6.39*	*6.41*	*1.19*
	7.90	7.90	7.90	0.00
Upper torso	*10.25*	*12.50*	*13.15*	*2.47*
	13.22	15.43	16.28	1.93
Lower torso	*26.27*	*25.55*	*25.01*	*4.74*
	33.89	31.54	30.84	1.74
Entire torso	*36.51*	*38.05*	*38.16*	*5.34*
	47.12	47.97	47.1	2.50
Torso + head	*42.64*	*44.44*	*44.57*	*5.48*
	55.0	54.9	55.0	2.50
Hand	*0.56*	*0.57*	*0.58*	*0.08*
	0.72	0.71	0.72	0.03
Upper arm	*2.51*	*2.66*	*2.65*	*0.65*
	3.23	3.28	3.23	0.18
Forearm	*1.47*	*1.54*	*1.54*	*0.33*
	1.89	1.91	1.90	0.05
Forearm + hand	*2.02*	*2.12*	*2.12*	*0.33*
	2.61	2.62	2.62	0.06
Upper extremity	*4.53*	*4.78*	*4.77*	*0.38*
	5.84	5.90	5.89	0.19
Thigh	*7.85*	*8.19*	*8.21*	*1.49*
	10.13	10.12	10.13	0.04
Lower leg	*3.92*	*4.13*	*4.12*	*0.90*
	5.06	5.10	5.06	0.15
Foot	*1.13*	*1.17*	*1.18*	*0.17*
	1.46	1.44	1.46	0.05
Lower leg + foot	*5.05*	*5.30*	*5.3*	*0.92*
	6.52	6.55	6.54	0.23
Lower extremity	*12.90*	*13.50*	13.51	1.75
	16.65	16.66	16.68	0.16

Table 1. Predicted segment weight (kg) and percentage of body weight for the two athletes in this study and the corresponding data of Miller and Morrison [46].

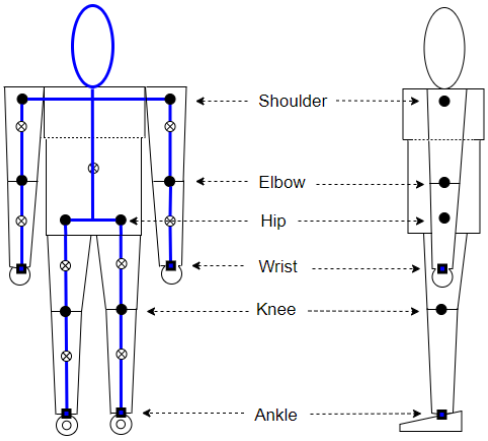

Figure 10. Front and side view of Woolley's model (not drawn to scale) with marked segment joints (closed circles) and local centres of gravity (open circles with a cross), and the wrists and ankles as distal points (closed squares) of the forearms and lower legs, respectively .

Woolley's model approximates nine body segments with specific geometric shapes for simplicity:

1. The head (included in segment 1) is approximated by a right circular ellipsoid;
2. The torso (included in segment 1) is approximated by a right elliptic cylinder;
3. The hands (included in segments 4 and 5) are approximated by spheres;
4. The upper arms (segments 2 and 3), the lower arms (segments 4 and 5), the upper legs (segments 6 and 7), the lower legs (segments 8 and 9), and the feet (included in segments 8 and 9) are all approximated by frustra of right circular cones.

Assuming uniform density, the local centre of gravity and the moment of inertia for each shape can be calculated. The centre of gravity is for most geometrical shapes in the middle of the shape is in the middle, except for the frustum of a cone. We do not expect that students derive formulas for computing moments of inertia about principle axes for the geometrical shapes used. Neither do we expect that they use the parallel axis theorem to compute moments of inertia of combined segments. They can simply lookup formulas, based on twenty-five anthropometric dimensions, in the supplementary file *Anthropometric model of man*. The supplementary JupyterLab notebook for Python [47] contains the programming code for the computations.

4.3 Results of computations for two athletes

This section presents the estimated segmental centres of gravities and the moments of inertia about principal axes for the two athletes in this study, compared with literature results.

Table 2 shows predicted centres of gravity as percentages of segment length (from proximal to distal) for both athletes, alongside average values and standard deviations from Miller and Morrison's summary of 30 male athletes [46]. Figure 11 visually represents the segmental centres of gravity for Athlete 1, along with the variables used in our computer programs for anthropometric computations. Such a visual aid is particularly useful for students.

Despite using basic tools to measure the twenty-five required anthropometric dimensions, the results for Athlete 2 closely match the literature values. Results of Athlete 1, however, show differences: The torso's centre of gravity is further away from the proximal endpoint, and the thigh's centre of gravity is closer to the proximal point. This highlights individual variations in body composition.

Differences between the athletes are more apparent in the segmental moments of inertia listed in Table 3. Athlete 1 has notably smaller moments of inertia for the upper torso segment than Athlete 2, while differences in other segments are much smaller. These values closely match those reported by Miller and Morrison [46].

The predicted centres of gravity (table 2), the estimated moments of inertia about principal axes (table 3), and the measured body segment lengths allow for the computation of radii of gyrations, listed in table 4 alongside those obtained by Dempster [48] (taken from [29]). Again, there is close align-

ment with values obtainable from data listed by Miller and Morrison [46]. However, the radii of gyrations for Athlete 1 are smaller (notably of the upper torso), suggesting a potential advantage in rotating this body part.

To explore this a bit further we compute moments of inertia of the human body about the transverse axis through the centre of gravity in five postures: (a) layout with hands stretched, downwards, (b) sideways, and (c) overhead, (d) pike, and (e) tuck (figure 12). The predicted values are listed in table 5.

Body part	Proximal / distal end	Athlete 1	Athlete 2	Miller & Morrison
Entire torso	Hip / Shoulder	53.6 / 46.4	44.3 / 55.7	44.0 / 46.0
Torso + head	Hip / Shoulder	67.9 / 32.1	59.3 / 40.7	58.2 / 41.8
Upper arm	Shoulder / Elbow	32.8 / 67.2	36.0 / 64.0	38.2 / 61.8
Forearm	Elbow / Wrist	43.4 / 56.6	44.9 / 55.1	42.7 / 57.3
Forearm + hand	Elbow / Wrist	65.0 / 35.9	65.5 / 34.5	62.7 / 37.3
Upper extremity	Shoulder / Wrist	48.6 / 51.4	50.5 / 49.5	47.6 / 52.4
Thigh	Hip / Knee	47.7 / 52.3	55.7 / 44.3	54.3 / 45.7
Lower leg	Knee / Ankle	42.2 / 57.8	43.0 / 57.0	41.9 / 58.1
Lower leg + foot	Knee / Ankle	56.9 / 43.1	57.5 / 42.5	56.4 / 43.6
Lower extremity	Hip / Ankle	45.2 / 54.8	47.7 / 52.3	50.0 / 50.0

Table 2. Predicted centres of gravity of body segments in percentage of segment length from proximal to distal endpoint for the two athletes in this study and the 'average athlete' of Miller and Morrison [46].

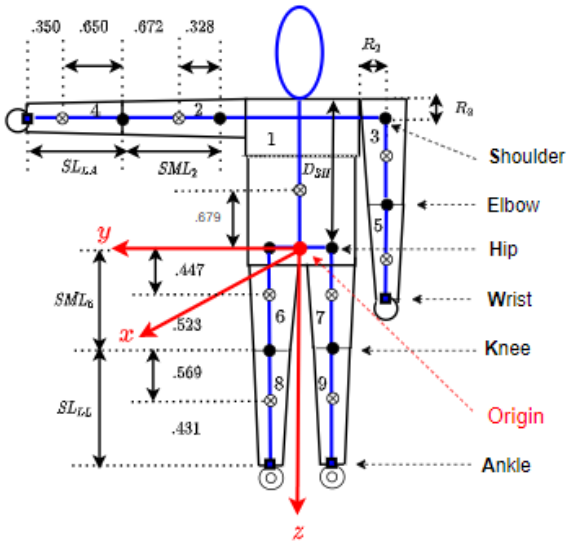

Figure 11. Body segment centres of gravity for Athlete 1 in Woolley's model of the human body.

Body part	Principal moment	Athlete 1	Athlete 2	Miller & Morrison Mean	Miller & Morrison Std. Dev
Head	I_{xx}, I_{yy}	0.0472	0.0471	0.0419	0.0104
	I_{zz}	0.0195	0.2033	0.0216	0.0047
Upper torso	I_{xx}	0.0964	0.1450	0.1544	0.0520
	I_{yy}	0.0572	0.0926	0.1055	0.0366
	I_{zz}	0.1177	0.1500	0.1382	0.0531
Lower torso	I_{xx}	0.5203	0.5736	0.5428	0.1753
	I_{yy}	0.4246	0.4512	0.4381	0.1453
	I_{zz}	0.2619	0.2914	0.2639	0.1028
Hand	I_{xx} , I_{yy}, I_{zz}	0.0005	0.0005	0.0005	0.0001
Upper arm	I_{xx}, I_{yy}	0.0266	0.0360	0.0296	0.0109
	I_{zz}	0.0035	0.0030	0.0032	0.0015
Forearm	I_{xx}, I_{yy}	0.0057	0.0068	0.0098	0.0033
	I_{zz}	0.0010	0.0009	0.0011	0.0004
Thigh	I_{xx}, I_{yy}	0.0952	0.0967	0.1024	0.0301
	I_{zz}	0.0250	0.0253	0.0273	0.0103
Lower leg	I_{xx}, I_{yy}	0.0517	0.0752	0.0684	0.0246
	I_{zz}	0.0050	0.0052	0.0056	0.0021
Foot	I_{xx}, I_{yy}	0.0063	0.0079	0.0075	0.0018
	I_{zz}	0.0004	0.0007	0.0005	0.0002

Table 3. Predicted moments of inertia ($\mathrm{kg} \cdot m^2$) of segments about the principal axes through the local centres of gravity.

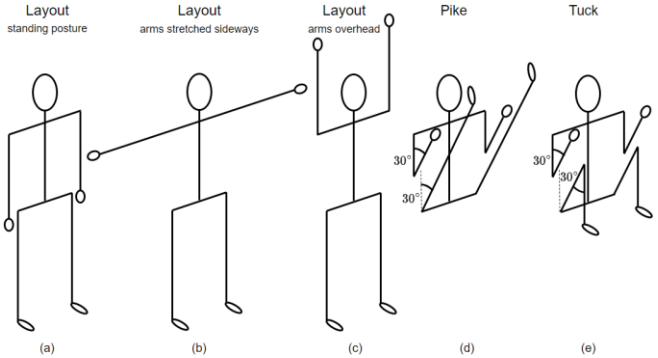

Figure 12. Five body postures relevant for competitive diving.

The estimated moments of inertia (in $\mathrm{kg} \cdot \mathrm{m}^2$) for the standing posture and the tucked posture in table 5 align with the values reported by Whittset [49]: 11.3 vs 12.3, and 3.4 vs 4.7, respectively. The inertia properties of Athlete 2 closely match those of the 'average athlete' of Miller and Morrison [46]. Athlete 1 consistently shows smaller moments of inertia across the five postures compared to Athlete 2. This suggests that Athlete 1 can rotate faster in any of these postures, given the same amount of angular momentum generated at take-off, providing a natural advantage for fast rotation.

Body part	Radius of gyration	Athlete 1	Athlete 2	Miller & Morrison	Dempster
Upper torso	ρ_{yy}	0.096	0.145	0.154	
	ρ_{yy}	0.057	0.093	0.106	
	ρ_{zz}	0.118	0.150	0.138	
Lower torso	ρ_{xx}	0.520	0.574	0.543	
	ρ_{yy}	0.425	0.451	0.438	
	ρ_{zz}	0.262	0.291	0.264	
Entire torso	ρ_{xx}	0.396	0.435	0.422	
	ρ_{yy}	0.371	0.410	0.402	
	ρ_{zz}	0.229	0.234	0.206	
Torso + head	ρ_{xx}	0.514	0.548	0.520	
	ρ_{yy}	0.498	0.531	0.506	0.503
	ρ_{zz}	0.218	0221	0.196	
Upper arm	ρ_{xx}, ρ_{yy}	0.356	0.336	0.348	0.322
	ρ_{zz}	0.129	0.097	0.115	
Forearm	ρ_{xx}, ρ_{yy}	0.296	0.295	0.290	0.303
	ρ_{zz}	0.125	0.108	0.098	
Forearm + hand	ρ_{xx}, ρ_{yy}	0.438	0.427	0.415	0.468
	ρ_{zz}	0.128	0.115	0.100	
Upper extremity	ρ_{xx}, ρ_{yy}	0.384	0.372	0.363	0.368
	ρ_{zz}	0.066	0.053	0.055	
Thigh	ρ_{xx}, ρ_{yy}	0.275	0.234	0.240	0.323
	ρ_{zz}	0.141	0.120	0.112	
Lower leg	ρ_{xx}, ρ_{yy}	0.287	0.287	0.287	0.302
	ρ_{zz}	0.089	0.076	0.089	
Lower leg + foot	ρ_{xx}	0.374	0.372	0.372	
	ρ_{yy}	0.384	0.380	0.383	0.416
	ρ_{zz}	0.118	0.106	0.121	
Lower extremity	ρ_{xx}	0.310	0.289	0.287	
	ρ_{yy}	0.311	0.291	0.288	0.326
	ρ_{zz}	0.066	0.057	0.059	

Table 4. Predicted radii of gyration (as proportion of segment length) of body segments about principal axes through the segments' centres of gravity.

Posture	Athlete 1	Athlete 2	Miller & Morrison
Layout (a)	11.3	14.0	14.5
Layout (b)	12.0	15.1	15.7
Layout (c)	14.3	18.5	18.9
Piked (d)	4.3	5.9	5.8
Tucked (e)	3.4	4.1	4.1

Table 5. Estimated moments of inertia ($\mathrm{kg \cdot m^2}$) of the whole body about the transverse axis through the centre of gravity in the five postures shown in figure 12 for the two athletes and the 'average athlete' of Miller and Morrison [46].

Another interesting aspect to explore is the contribution of each segment to the total moment of inertia, considering both the local and remote terms. Recall that the local term represents the moment of inertia of a segment about an axis through its centre of gravity. The remote term, derived from the parallel axis theorem, is the product of the segment mass and the square of the perpendicular distance between the parallel axes. Question is whether one of the terms can be ignored under circumstances, simplifying computations.

Table 6 lists the percentage of the total moment of inertia about the transverse axis for each segment in Woolley's model [41], along with the percentage of the local term's contribution for each posture shown in figure 12, for the 'average athlete' of Miller and Morrison [46]. The table provides the following key insights. In general, the local moment of inertia of segments are significant in computing the total moment of inertia. The torso+head segment and the lower extremities together contribute 90% up to 95% of the total moment of inertia in all postures, except when the arms are overhead. This suggests that the upper extremities can be ignored when estimating the total moment of inertia in a piked posture, simplifying computations. Actually, the estimated moment of inertia for the piked posture of the 'average athlete' in figure 12 using only the torso-head segment and the lower extremities is equal to 5.6 $\mathrm{kg \cdot m^2}$, and hardly differs from the value of 5.8 $\mathrm{kg \cdot m^2}$, when the arms are included in the computation.

Body parts	Layout (a)	Layout (b)	Layout (c)	Pike (d)	Tuck (e)
Torso + head	38.5 48.6	31.2 55.3	22.8 62.8	53.3 87.8	70.4 93.3
Upper arms	4.7 8.3	6.2 0.6	7.6 4.0	1.8 55.9	3.2 42.7
Forearms + hands	0.4 99.1	4.9 0.4	17.0 1.7	0.9 99.2	1.8 73.8
Upper extremities	5.1 15.0	11.1 0.5	24.5 2.4	2.7 71.0	5.0 53.7
Thighs	12.1 13.7	13.3 11.5	13.0 9.7	7.5 55.6	8.4 69.4
Lower legs + feet	44.3 3.9	44.3 3.6	39.7 3.4	36.5 12.0	16.2 37.9
Lower extremities	56.4 6.0	57.7 5.5	52.7 5.0	44.0 19,4	24.6 48.6

Table 6. Contributions of segments (in percentage) to the total moment of inertia about the transverse axis through the centre of gravity for the 'average athlete' of Miller and Morrison [46] and the local term in each contribution (in percentage).

The local and remote terms of the total moment of inertia can be defined as the sum of the local terms and the sum of the remote terms of the segmental moments of inertia, respectively. Table 7 lists the contributions of the local and remote term to the total moment of inertia (in percentage) for each posture shown in figure 12 for the 'average athlete' of Miller and Morrison [46]. It is evident that the local term plays a more significant role when the athlete is in a piked or tucked posture compared to a layout posture. This aligns with expectations, as the extremities are closer to the body's centre of gravity in these postures.

Term	Layout (a)	Layout (b)	Layout (c)	Pike (d)	Tuck (e)
Local	22.8	20.5	17.5	57.3	80.3
Remote	77.2	79.5	82.5	42.7	19.7

Table 7. Contribution of each term (in percentage) to the total moment of inertia about the transverse axis through the centre of gravity for the 'average athlete' of Miller & Morrison [46].

5. Motion analysis of a 107B dive

Analysing somersaults in diving via video is more complex than it might initially appear. Mikl [15], Sayyah [50], and Sotheran [51] describe in great detail how they collected and analysed data obtained with equipment ranging from an expensive high-speed camera to a low-cost point-and-shoot camera, recording at a framerate of 120 up to 250 fps in high resolution. They detail the challenges they faced in a video-based method for obtaining kinematic data. They used various tools for digitisation, ranging from custom-made software to low-tech options like Tracker [52]. Key issues include camera positioning to capture the entire motion with minimal camera distortion, lighting for high-speed recording, dealing with swimming pool climate conditions, camera calibration for accurate screen-to-world coordinate conversion, using multiple cameras for recording 3D motion, manual digitisation of body landmarks versus automatic tracking, choosing appropriate markers, and managing occlusion. These factors significantly impact data accuracy.

Despite these challenges, students can still collect kinematic data of a quality that is good enough to explore the physics of diving. Also the fact that we use low-tech tools to measure anthropometric data of the athletes in order to estimate various centres of gravity and inertia properties of individual athletes does not seem to affect the quality of the results. The main difficulty we encountered was with automatic tracking of body markers. Even with multi-coloured kinesiology tape markers, automatic tracking often required manual corrections due to background interference and occlusion, making the process error prone. As a result, we opted in favour of manual digitisation, accepting its time-consuming nature and potential for digitising errors. After reading the PhD thesis of Sotheran [51], we realise that we had simply been too optimistic about automatic tracking of the athlete's motion from take-off to water entry. Also Mikl [15] reports about manual adjustments of mistakes needed in object tracking.

In the rest of this section we present a video analysis of a 107B dive recorded at a frame rate of 100 fps and resolution of 1920x1080. In this analysis, we assume that the arms and legs of the athlete are straightened and move parallel after take-off, maintaining left-right symmetry. This reduces the model to three rigid bodies: the torso+head segment, a pair of lower extremities, and a pair upper extremities. Thus, we only need to collect position data for four key points: ankle, hip, shoulder, and wrist joint, each marked with kinesiology tape.

Not all body segments in the 107B dive move in the two-dimensional plane of motion: When the athlete is in a piked posture, he has his hands wrapped around the legs (near the back of the knee). We simply ignore this and use the shoulder and the visible part of the arms as key points for the upper extremity. We justify this simplification by the small contribution of upper extremities to the total moment of inertia in comparison to the other two body parts (see table 6).

After collecting position data of the four key points, the graphs of the horizontal and vertical coordinates over time for each key point are checked to correct any small errors in the digitisation. In addition, noise reduction of the data before starting a data analysis can be done in COACH [6,7] via a generalised cross-validatory penalised cubic spline-smoothing algorithm [33]. This significantly improves results.

5.1 Estimation of the centre of gravity, somersault angle, and angular velocity

A key step in video analysis is computing the athlete's centre of gravity (CG) position during flight, along with the somersault angle α, and the angular velocity ω (defined as the time-derivative of α). Figure 13 depicts a snapshot of this analysis, covering a 107B dive from take-off to water entry.

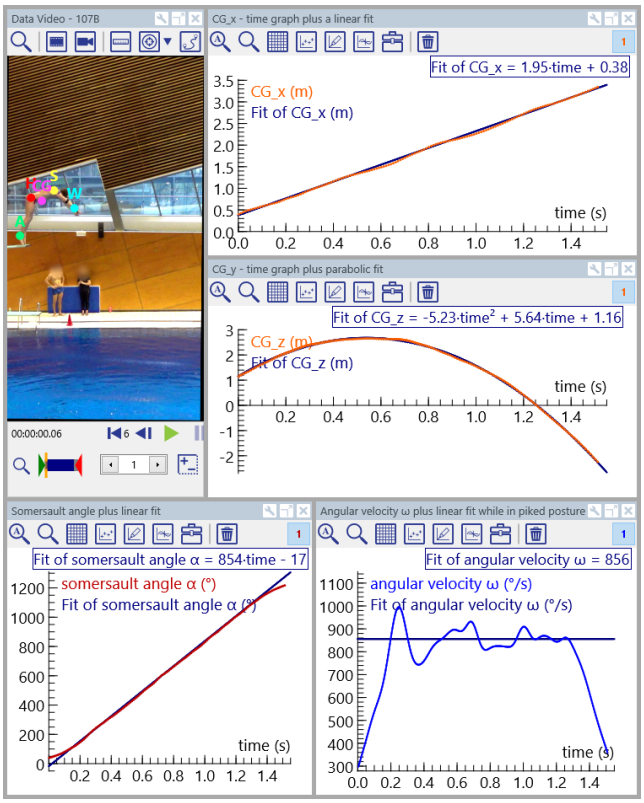

Figure 13. Screenshot of a video analysis in which the time course of the centre of gravity, the somersault angle, and the angular velocity of an athlete are estimated while he is airborne in a 107B dive.

To the right of the video window, which has been slightly rotated (2.7°) in COACH to align the digital coordinate system with the real-world horizontal and vertical directions, graphs of the x- and z-coordinates of the estimated centre of gravity (CG) are displayed. A linear fit of the x-coordinate over time indicates that CG moves horizontally at a constant speed of 1.95 m/s. A parabolic fit of the z-coordinate, i.e. the vertical coordinate, shows a vertical initial speed v_z of 5.65

m/s. From this value one can compute the flight height h_{flight}, defined as the difference between the maximum height of CG and the height of CG at take-off, via the formula

$$h_{\text{flight}} = \frac{v_z}{2g}.$$

Using for the acceleration of gravity g the value it would have according to the parabolic curve fit, i.e. $g = 10.46\ \text{ms}^{-2}$, we get a flight height of 1.51 m. This is much more than an athlete could achieve when jumping from standing position of the floor: The springboard really contributes to achieving height. Using the built-in ruler in the video window, we measure the same value. Trusting the ruler, it is easy to measure the dive height h_{dive}, defined as the difference between the maximum height of CG and the height of CG at water entry: In this way we get $h_{\text{dive}} = 4.81$ m.

Flight time t_{flight}, defined as the time from the last instant of take-off, when the feet leave the springboard, until the athlete enters the water, can be calculated using

$$t_{\text{flight}} = \frac{v_z + \sqrt{{v_z}^2 + 2g\left(h_{\text{CG,take-off}} + h_{\text{CG,entry}}\right)}}{g},$$

where $h_{\text{CG,take-off}}$ and $h_{\text{CG,entry}}$ are the heights of CG at the last instant of take-off and at the first instant of water entry, respectively. This results in a flight time of 1.51 s, a value that can also be read off from the time graph of v_z by scrubbing the video, i.e. by advancing or reversing a video clip manually for the purpose of precisely identifying and marking interesting events in the movie and to relate them with graphical features (e.g. coordinates of key variables).

The somersault angle α can be computed via the slope of a line between the centres of gravity of the lower extremities and the torso+head segment, and via step functions making the somersault angle continuous. The graph of the somersault angle (lower-left window in figure 13) is nearly linear in a piked posture, with a constant angular velocity ω of 854 °/s from a linear regression. The pieces of the graph at the start and end of the dive suggest lower angular velocities just after take-off and just before water entry. The graph of the angular velocity (lower-right window in Figure 13), computed using a penalised smoothing algorithm in COACH [6,7], shows a similar value of 856 °/s, confirming the initial results.

We mention these possibilities of calculating or measuring kinematic variables for a dive because they are tasks helping students experience that many variables can be estimated through various methods, promoting accuracy and reliability in their analyses, and that contextual graphs usually contain much information about events visible in a video clip.

5.2 Angular velocities of body segments

For deeper understanding of body motion during a 107B dive, analysing the angular velocities of body segments is essential. Figure 14 includes annotated graphs of the computed angular velocities for the arms, torso+head, and legs. The scanning mode is fixed at the instant the piked posture opens.

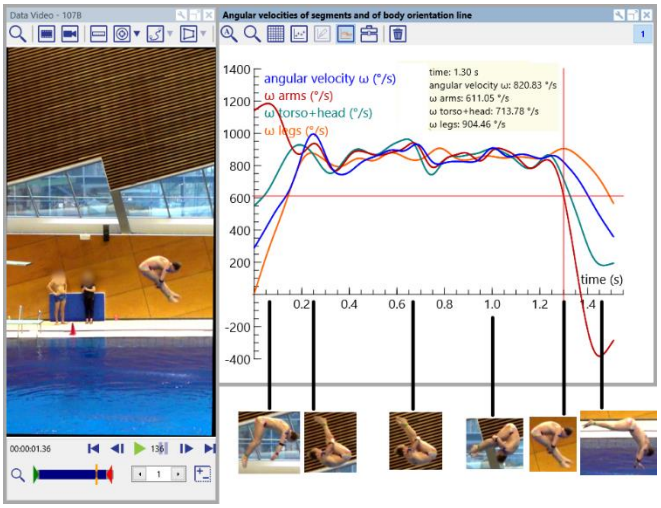

Figure 14. Screenshot of a video analysis showing the time courses of the angular velocities of segments and the total body during a 107B dive. The screenshot is annotated with images of body postures at key events during the flight. The video captures the athlete opening a piked posture in preparation for entering the water.

The graphs show that the arms rotate quickly downward at the dive's beginning, a motion that starts during the last phase of take-off while the athlete is still in contact with the springboard, and then slows down. The torso+head segment also rotates fairly rapidly, with its angular velocity increasing as the athlete transitions to a piked posture. Initially, the lower extremities rotate slower than other segments but soon catch up, with all segments reaching and fluctuating around a constant angular speed of 850 °/s. This indicates that in a piked posture, the athlete's segments move together, and their angular velocities align with the total body's angular velocity estimated as the rotation of the chosen line of body orientation. As the athlete prepares for water entry, the graphs reveal that the rotation speed of the arms and torso+head segment decreases first, followed by a reduction in the legs' rotation speed. This observation is verified in the next subsection.

When students do a similar video analysis of a dive and analyse graphs similar to the ones shown in figure 14, they experience that it makes sense to divide the dive flight into differing phases, and that graphs provide detailed information about segmental body motions in a real diving context, which might be challenging to discern directly from a video clip.

5.3 The shape angles of hip and shoulder

Key kinematic variables for the 107B dive are the shoulder-hip-ankle angle and the wrist-shoulder-hip angle, also known as the hip and shoulder shape angles, respectively. These angles can be computed using the cosine rule. For example, the hip shape angle is calculated as

$$\text{hip shape angle} = \arccos\left(\frac{{d_{HA}}^2 + {d_{HS}}^2 - {d_{AS}}^2}{2 d_{HA} d_{HS}}\right),$$

where d_{HA} is the distance between hip and ankle joint, d_{HS} is the distance between hip and shoulder joint, and d_{AS} is the distance between ankle and shoulder joint. This formula underscores again the importance of mathematics in physics explorations.

Figure 15 shows annotated graphs of these shape angles, fixed at an instant when the athlete apparently reinforces the piked posture by bending the hips further. The graphs reveal that arm bending precedes hip bending as the athlete moves into the piked posture at the start of the flight. The opening of the piked posture coincides with simultaneous increases in both shape angles, demonstrating that the athlete uses the straight-line come-out technique (see [53, 54]). This technique is mostly used when there is not a lot of time anymore to prepare the water entry.

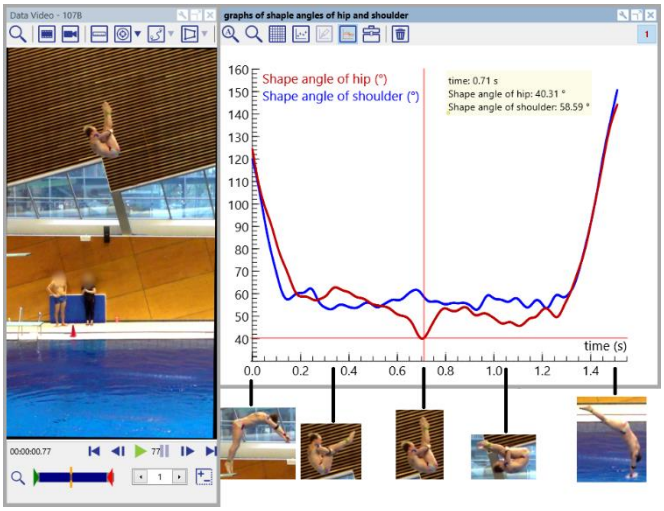

Figure 15. Screenshot of a video analysis showing the time courses of the hip and shoulder shape angles during a 107B dive. The picture is annotated with images of body postures at key moments during the flight. The video captures the athlete's deepest piked posture, highlighting the strong bend at the hips.

5.4 Moments of inertia of segments and the total body

Moments of inertia of segments and the total body can be estimated at any time during flight using the formulas of Woolley's model of the human body [41]; see section 4 and the supplementary file *Anthropometric model of man.*

Figure 16 shows graphs of these estimated moments of inertia while the athlete is airborne in the 107B dive. It is clear that the moment of inertia of the arms is small compared to the legs and torso+head while the athlete is in a piked posture. The estimations show that in a piked posture, the moments of inertia of the legs and torso+head are almost equal. The graphs illustrate how the athlete decreases his moment of inertia via the piked posture, allowing for faster rotation: In $\text{kg} \cdot \text{m}^2$, it goes from 16.7 at take-off to 6.5 in the piked posture, and ends at 17.9 in the layout posture with arms overhead. These values are higher than those computed for Athlete 1 in section 4.3, likely due to the length calibration in the video analysis. The vertical distance was estimated at 3 meter using the tip of the springboard at rest and the splash point at water entry. Despite small calibration errors, our estimated quantities align with values reported in research literature (e.g. table 2.2. in [55])

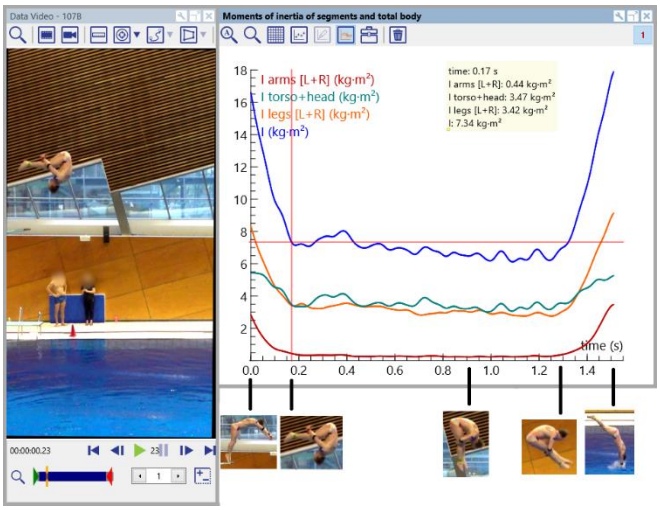

Figure 16. Screenshot of a video analysis showing the time courses of the moments of inertia of segments and total body during a 107B dive. The picture is annotated with images of body postures at key moments during the flight. The video captures the athlete starting the piked posture.

5.5 Angular momenta of segments and the total body

As mentioned in the introduction, we aim to verify that the angular momentum of the athlete's body, obtained at take-off, remains constant while airborne. We also explore methods for estimating the angular momenta of segments and the total body, distinguishing between local and remote components. We write "estimating" instead of "computing" to emphasise that there is no exact calculation of the moment of inertia of the human body; one can only determine approximate values.

In section 2.4, we discussed two methods for estimating angular momenta. The first method uses a line of body orientation and the formula $L = I \cdot \omega$, where I is the moment of inertia about the transverse axis through the body's centre of gravity and ω is the angular velocity of the somersault angle. This method is approximate and works only when the shape angles of the hip and shoulder do not change.

The second method estimates angular momentum about the transverse axis through the centre of gravity via a formula that is also correct when shape angles of hip and shoulder change. It consists of a local term (sum of angular momenta of segments about transverse axes through their centres of gravity) and a remote term (sum of angular momenta of the segmental centres of gravity about the transverse axis through the body's centre of gravity).

Figure 17 shows the time course of the angular momentum of the athlete's body about the transverse axis through the centre of gravity, estimated by both methods. When the athlete is in a piked posture, the two graphs are similar and can be approximated by a horizontal regression curve with a constant value of 102 $\mathrm{kgm^2s^{-1}}$. The second method's graph aligns with this curve throughout the flight, illustrating the law of conservation of angular momentum. Given the necessary derivatives and assumptions (section 5.1), this is a good result.

Figure 17 also includes the graphs of the local and remote terms of the total angular momentum L. It shows that both terms significantly contribute to the total angular momentum. The local term is largest in a piked posture and smallest in layout postures at take-off and water entry, consistent with the results in Table 7 for an 'average 'athlete.

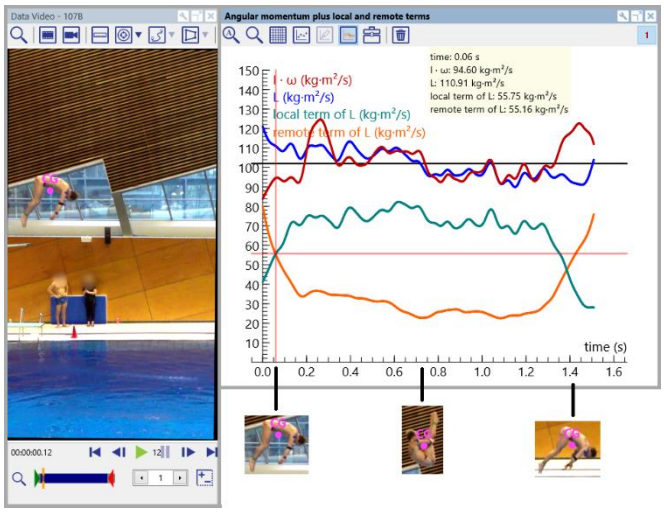

Figure 17. Graphs of the total angular momentum L while the athlete is airborne in a 107B dive, estimated by two methods: $L = I \cdot \omega$ (red curve) and $L = L_{\mathrm{local}} + L_{\mathrm{remote}}$ (blue curve), where $L_{\mathrm{local}} = \sum_s I_s \cdot \omega_s$ and $L_{\mathrm{remote}} = \sum_s m_s \cdot [\vec{r_s} \times \vec{v_s}]_3$. The horizontal black line indicates the best constant angular momentum L. The left and right annotations show postures when the local and remote terms are equal, while the middle annotation shows the posture with a minimal remote term.

Figure 18 shows the graphs of the angular momenta of segments and total body while the athlete is airborne in a 107B dive. It is evident that the arms have substantial angular momentum at take-off, as the athlete is still swinging his arms rapidly towards his torso. Once the shoulder angle is fixed and the athlete is in a piked posture, the angular momentum of the arms becomes negligible. In this posture, the contributions of the torso+head segment and the legs to the angular momentum are nearly equal. This aligns with the earlier finding (figure 16) that these segments contribute similarly to the total moment of inertia.

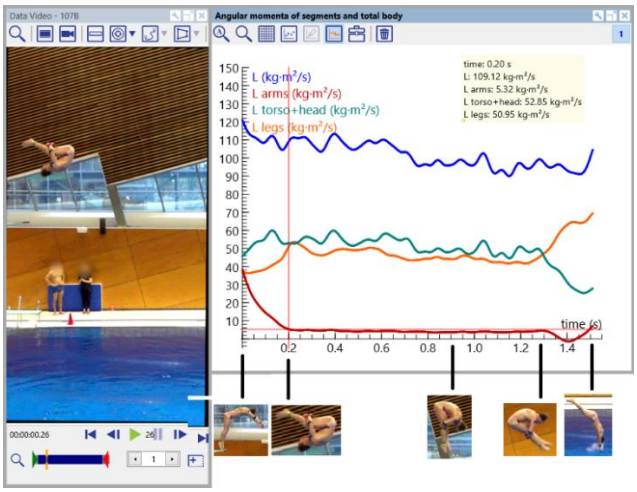

Figure 18. Graphs of angular momenta of segments and total body while the athlete is airborne in a 107B dive. The video captures the start of the piked posture of the athlete.

6. Motion analysis of a 105B dive

Motion analysis becomes more insightful when comparing different body movements. To this end, we carry out a similar video analysis as in the previous section, but for a 105B dive of the same athlete, i.e. a forward two-and-a-halve somersault in a piked posture. Now, the angular displacement of the athlete is less, and we aim to explore the impact on performance.

6.1 Video analysis of a 105B dive

Figure 19 shows a screenshot of a video analysis estimating the centre of gravity (CG), the somersault angle, and the angular velocity during a 105B dive. The athlete's CG follows a parabolic trajectory, but with a horizontal speed of 1.11 m/s —less than in the 107B dive—while the initial vertical speed of 6.27 m/s is greater. This indicates a more vertically directed jump at take-off compared to the 107B dive, as reflected in the video window of figure 19, where the athlete leans less forward than in the captured posture in figure 13. Consequently, he generates less angular momentum at take-off, resulting in a lower angular velocity of approximately $\omega \approx 673^{\circ}/s$ during the piked posture time interval (0.25, 0.86).

Interestingly, in this dive, after deceleration due to opening the piked posture, there is a temporary increase in angular velocity as the athlete prepares for water entry. Walker [56, figure 9] observes a similar pattern, suggesting it might be "due to the shoulders adducting after initial abduction, resulting in a reduction in the mass moment of inertia, in preparation of the straight arm line for water entry." However, in our video, we notice that the athlete temporarily bends his hips more strongly, from a hip shape angle of 89° at 3 o'clock position of his legs to 82° at 6.30 o'clock position of his legs (as shown in figure 20 at times 1.06s and 1.32s, respectively), reducing the moment of inertia and thus increasing angular velocity.

Figure 20 presents annotated graphs of the computed angular velocities for the arms, torso+head, and legs. The temporary increase in angular velocity of the hip+torso segment and the legs when the athlete prepares for water entry is visible. At the local maximum, shown in a still image below the horizontal axis, the hip shape angle is 82°. The athlete begins opening the pike posture by removing his hands from his legs and abducting his arms to the side when his legs are at 10 o'clock position. He maintains the piked posture, reaching a local minimum of angular velocity with his legs at 2 o'clock position. The angular velocities of the segments and the total body remain nearly constant during the time interval (0.25,0.86).

The extra bending of the hips while the athlete prepares for water entry is also visible as a little dip in the graph of the hip shape angle near the end of the flight, shown in figure 21. What catches the eye in figure 21 is the 'spike' in the graph of the shoulder shape angle, due to rapid motion of the arms downward followed by a rapid motion to get them overhead. The reason for having the arms close to the body at an instant during flight could be to aesthetically please a judge by showing the pike posture more clearly. However, a better reason for using this so-called pike-out come-out technique [53,54] is that it allows more time to see the entry point and more opportunity to adjust the water entry, when the body is straightened and the arms are brought overhead.

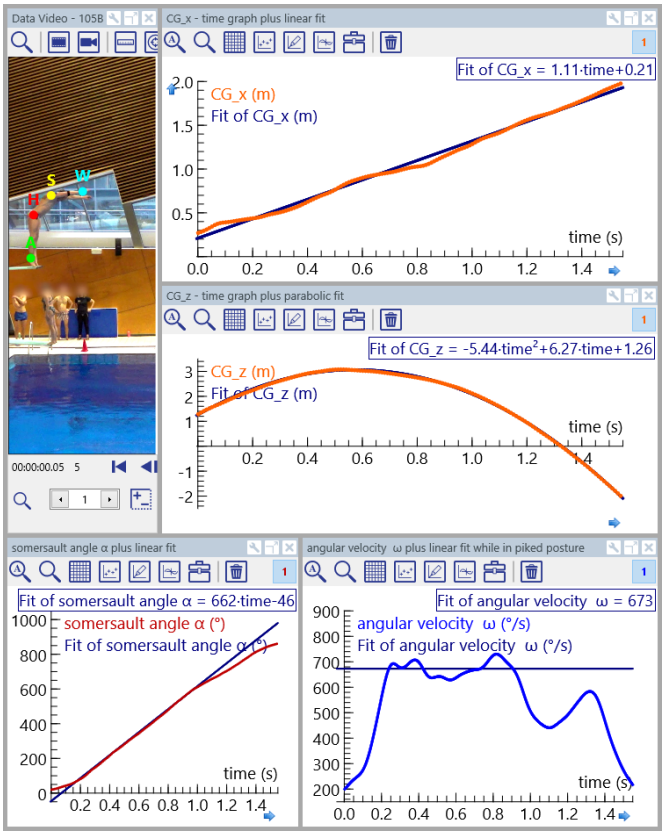

Figure 19. Screenshot of a video analysis estimating the centre of gravity, the somersault angle and the angular velocity of an athlete during a 105B dive.

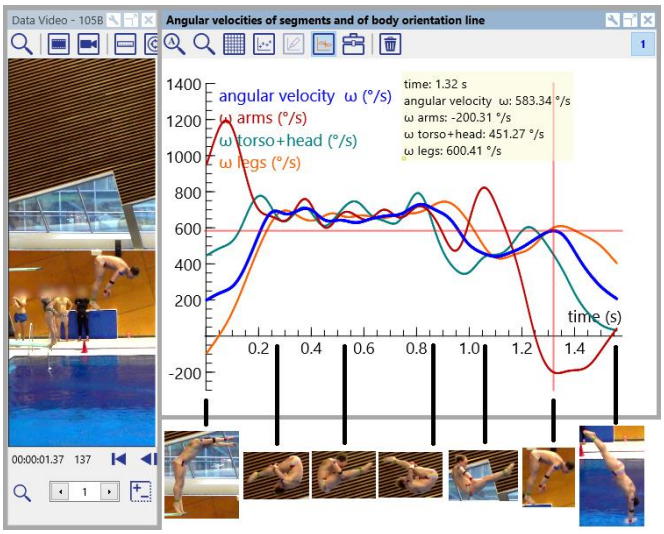

Figure 20. Screenshot of a video analysis showing the time courses of the angular velocities of segments and the total body during a 105B dive.

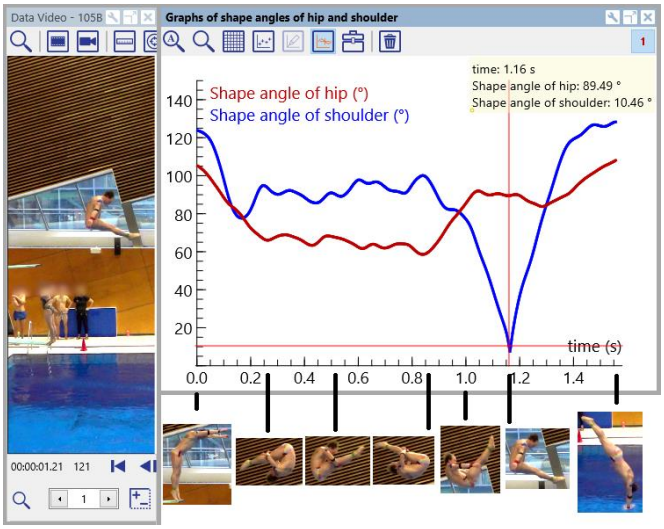

Figure 21. Screenshot of a video analysis showing the time courses of the hip and shoulder shape angles during a 105B dive.

Figure 22 shows graphs of estimated moments of inertia about the transverse axis through the centre of gravity while the athlete is airborne in the 105B dive. The temporary dip in the moment of inertia near the end when the athlete is preparing for water entry is visible, and is caused by a dip in the moment of inertia of both legs and the torso+head segment.

Figure 23 shows the time course of the athlete's angular momentum about the transverse axis through the centre of gravity, estimated by the two methods described in section 2.4. The graphs of the local and remote terms of the total angular momentum L are included. Both terms significantly contribute to the total angular momentum. The local term is largest in a piked posture and smallest in the layout postures at take-off and water entry, consistent with earlier results. The video stills

below the diagram illustrate that the local and remote terms are equal in an open piked posture with a hip shape angle close to 90°. Recall that figure 23 was also created to explore the law of conservation of angular momentum. The blue graph, computed with the accurate method (see section 2.4), shows that the estimated angular momentum L remains, as expected, nearly constant throughout the flight phase, having a value of 75 $\mathrm{kgm^2s^{-1}}$. The angular momentum is lower in a 105B dive than in a 107B dive because the athlete does not need to rotate as quickly.

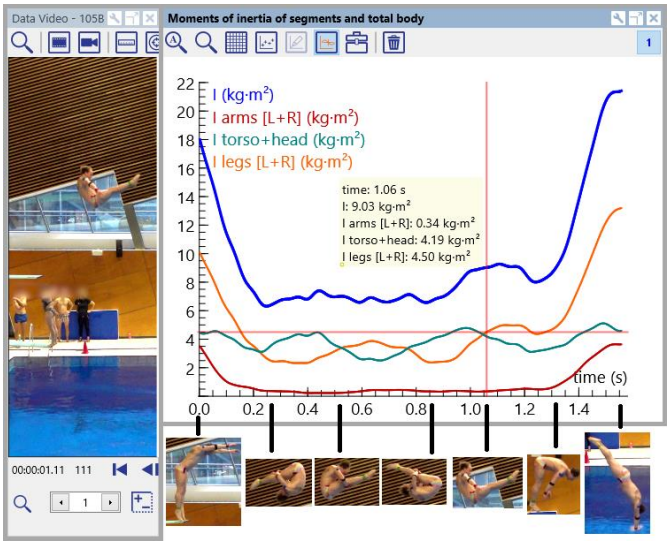

Figure 22. Screenshot of a video analysis showing the time courses of the moments of inertia of segments and total body during a 105B dive.

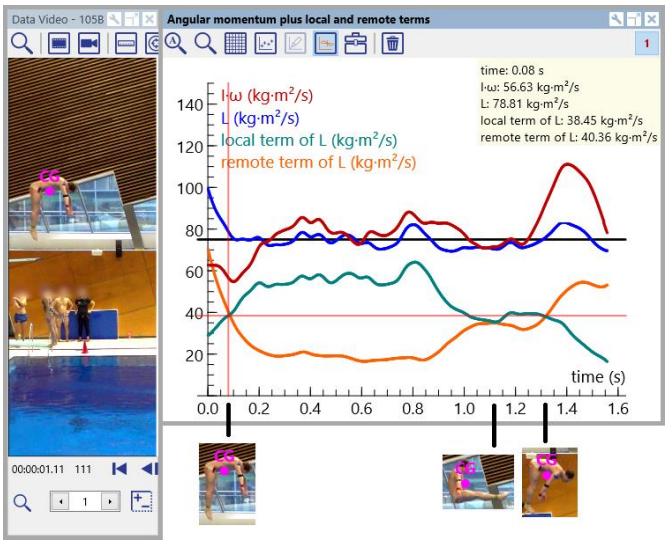

Figure 23. Graphs of the total angular momentum L while the athlete is airborne in a 105B dive, estimated by two methods (see section 2.4). The horizontal black line indicates the best constant angular momentum L

6.2 Estimating kinematic measures

Simpler student activities include estimating and comparing kinematic measures such as dive height, body orientation angle, hip and shoulder angles at take-off and water entry, total flight time, and angular displacement during the dive. For these activities, it suffices to collect position data of some key points of the human and create graphs of the time course of kinematic variables. Scrubbing video clips and simultaneously observing key events in the graphs, recording the times when they occur, and using digital measurement tools like a ruler and protractor in the video analysis environment is all what is needed. The required mathematical skills in such activities is kept at upper-secondary level when one uses an easily marked line of body orientation for the somersault angle, for instance, the line through the knee and the shoulder. Advantage of such activities is that they let students think about how to define the kinematics variables and how to measure or estimate them.

Table 8 lists definitions for three flight phases: initial flight, somersault, and opening. Other definitions are possible for body alignment, but may rely on more complex kinematic variable estimations.

Measure	Definition
Total flight	From final frame of foot contact with the springboard, take-off, to the first frame where hands break the water on entry
Initial flight	From take-off to the first frame where the hands touch the legs to form the somersault posture
Somersault	From the formation of the somersault posture to the first frame where the hands leave the legs, opening
Opening	From opening of the somersault posture to the first frame where hands break the water on entry
Take-off body alignment (°)	Angle of the line through knee and shoulder with the vertical axis at take-off
Entry body alignment (°)	Angle of the line through knee and shoulder with the vertical axis at take-off
Take-off hip angle (°)	Included angle between leg and torso at take-off
Entry hip angle (°)	Included angle between leg and torso at hand entry
Take-off shoulder angle (°)	Included angle between arm and torso at take-off
Entry shoulder angle (°)	Included angle between arm and torso at hand entry
Total flight duration (s)	Duration from take-off to hand entry
Total flight angular displacement (°)	Total rotation achieved by the body orientation line from take-off to hand entry

Table 8. Definition of the dive flight phases and some kinematic measures.

Table 9 lists some kinematic measures for the 105B and 107B dives. From the values obtained, we conclude that in a 107B dive, compared to a 105B dive, the athlete leans more

forward at take-off (larger take-off body alignment) by bending more his hips (smaller take-off hip angle). This leads to a less high dive and consequently to a smaller total flight time. The athlete has thrown his arms more rapidly downwards at take-off (smaller take-off shoulder angle). At water entry, the athlete's body is less straightened into layout posture (smaller entry hip and shoulder angle) and is less vertically oriented (smaller entry body alignment). The athlete has not enough time to complete the three-and-a-halve somersault: He misses angular displacement for a good water entry (smaller entry body alignment). The total flight angular displacement is always less than the specified angular displacement because of leaning at take-off, but in the 107B dive 87° is missing (compared to 55° in the 105B dive). So, stories can be told not only with graphs, but also with tables! This data-based storytelling approach encourages students to think critically about kinematic variables and their measurements.

Measure	105B	107B
Take-off body alignment (°)	23	43
Take-off hip angle (°)	141	123
Take-off shoulder angle (°)	139	120
Entry body alignment (°)	148	136
Entry hip angle (°)	168	140
Entry shoulder angle (°)	153	147
Total flight duration (s)	1.55	1.50
Total flight angular displacement (°)	845	1173

Table 9. Measured quantities for the 105B and 107B dive.

7. Conclusion

This paper explores opportunities for upper-secondary students and beyond to delve into angular kinematics and angular kinetics in the context of springboard diving at various levels of difficulty. It highlights the ICT-supported interaction between the world of phenomena, in which empirical data is collected and analysed, and the world of theories, in which ideas are scientifically developed and further explored (cf. [57,58]. In this case, the world of phenomena involves video recording of springboard dives and motion analysis using the versatile COACH environment [6,7] for STEM education. This authoring environment provides tools for measurement on digital videos (e.g., collecting position data, measuring length and angles, adjusting properties of a video), for data processing and analysis of data (e.g. differentiation, data smoothing, regression analysis), and for data visualisation in sync with the video clips, enabling quantitative exploration of human movement. The world of theories consists here of angular kinematics, angular kinetics, and mathematical modelling of the human body. The student investigations presented aim to deepen understanding of concepts like moment of inertia and angular momentum by connecting them to the real context of planar somersaults in springboard diving. Students learn to estimate moments of inertia using mathematical models of the human body. We adhere to the advice of Laws and Pfister [23]: "We recommend that this type of angular momentum conservation project be undertaken only by capable, highly motivated students." This certainly holds for the more advanced activities of using mathematical models to estimate moments of inertia and angular momenta. Students will need advice and guidance from their physics teachers. We hope and expect that these teacher are supported by the background information provided in this paper and its supplementary files.

We end this section with some remarks about the authentic nature of the student activities and why we consider it important. What we see as main goal of the inquiry activities presented is that they give students the opportunity to

- work with real data collected from video clips, preferably captured by themselves in a setting they have created themselves (they can certainly perform dives with low number of half somersaults, and they will have more interest and fun in analysing movements of themselves or friends);
- carry out practical work in which they can apply much of their present knowledge of mathematics and physics in a challenging real-life context;
- practice ICT skills, in particular making useful video clips, and doing data processing and video analysis;
- experience that diagrams that are used in practice are not just pretty pictures, but contain much information about the real-life phenomenon under study;
- interpret and theoretically underpin results;
- engage with modern research in movement science, including its terminology and methods.

Important research abilities that students practise through this kind of practical investigations are:

- formulate good research questions that guide the work;
- linger upon useful definitions of kinematic variables;
- design and implement an experiment for collection of relevant data;
- apply mathematical knowledge and techniques, and science concepts in new situations;
- effectively use a computer in research work;
- construct, test, evaluate, and improve methods for analysing data, and have insight in their role in science;
- interpret, theoretically underpin and reflect on results;
- collaborate with others in an investigation task.

ICT plays an important role in enabling students to carry out investigations at a high level of quality. It also brings the real world into mathematics and physics education in an attractive way. Learning and doing physics may be more fun in this approach than traditional teaching via lectures and practice sessions.

We interpret the authentic nature of the investigation as the opportunity for students to work directly with high-quality,

real-time data about springboard, much like movement scientists. This approach aims to make their learning and application of mathematics and science resemble real-world practice, characterised by being challenging, complex, open-ended, and cross-disciplinary, requiring a strong commitment and a broad range of skills (cf. [59]). The alignment of experiments, theory, and experiential knowledge is particularly rewarding, as demonstrated in this study on the biomechanics of springboard diving, with the quantitative verification of the law of conservation of angular momentum during the flight phase of dives in a piked posture as one of the highlights. Yet, the experimental design and modelling, the underlying thinking processes, discussions with peers, the effective use of ICT, and the improvement of students' mathematical and scientific literacy promoted by student-driven investigations are more important than the result obtained.

References

[1] Giancoli D 2014 *Physics – Principles with Applications* (7th ed.) Pearson

[2] Townend S 1993 Modelling the gymnastics giant swing – Is it potentially dangerous? *Tech. Math. Appl.* **12** 163-5 https://doi.org/10.1093/teamat/12.4.163

[3] Heck A, Knobbe D, Nijdam N, Slooten O and Uylings P 2011 Exploring the giant circle on the high bar with ICT tools. In: Joubert M, Clark-Wilson A and McCabe M (eds.) *Enhancing Mathematics Education Through Technology* (Proc. ICTMT10, Portsmouth, UK: University of Portsmouth) pp. 134-40

[4] Contakos J, Carlton L, Thompson B and Suddaby R 2009 The physics of a gymnastics flight element *Phys. Teach.* **47** 355-61 https://doi.org/10.1119/1.3204116

[5] Page R 1976 The mechanics of swimming and diving *Phys. Teach.* **14** 72-80 https://doi.org/10.1119/1.2339314

[6] Heck A, Kedzierska E and Ellermeijer T 2009 Design and implementation of an integrated computer working environment *J. Comput. Math. Sci. Teach.* **28** 147-61

[7] Heck A 2012 Perspectives on an integrated computer learning environment *Doctoral Thesis* University of Amsterdam (available at: https://dare.uva.nl/record/409820)

[8] Miller D and Munro C 1985 Greg Louganis' springboard takeoff: I: temporal and joint position analysis. *Int. J. Sport Biomech*. **1** 209-20

[9] FINA technical diving committee 2020 *FINA Diving Officials Manual* www.fina.org

[10] Rewt D 1993 Movement control in springboard diving *PhD thesis* University of Edinburgh (available at http://hdl.handle.net/1842/6962)

[11] Kong P 2005 Computer simulation of the takeoff in springboard diving *PhD Thesis* University of Loughborough (available at https://hdl.handle.net/2134/9051)

[12] Barris C 2013 An examination of learning design in elite springboard diving *PhD thesis* Queensland University of Technology (available at https://eprints.qut.edu.au/63807/)

[13] Haake S, Goodwill S, Heller B, Schorah D and Gomez J 2010 Dynamic modeling of a springboard during a 3 m dive *Procedia Eng.* **2** 3299-304 https://doi.org/10.1016/j.proeng.2010.04.148

[14] Demestre L, Grange S, Dubois C, *et al* 2022 Characterization of the dynamic behavior of a diving board using motion capture data *Sports Eng.* **25** 21 https://doi.org/10.1007/s12283-022-00388-z

[15] Mikl J 2015 All spun out *PhD thesis* University of Sidney (available at https://hdl.handle.net/2123/15375)

[16] Yeadon M 1984 The mechanics of twisting somersaults *Doctoral Thesis* University of Loughborough (available at https://hdl.handle.net/2134/7502)

[17] Rimoldini L and Singh C 2005 *Phys. Rev. ST Phys. Educ. Res.* **1**, 010102 https://doi.org/10.1103/PhysRevSTPER.1.010102

[18] Close H and Heron P 2011 Student understanding of the angular momentum of classical particles *Am. J. Phys.* **79** 1068-78

[19] Barniol P, Zavala G and Hinojosa C 2013 Students' difficulties in interpreting the torque vector in a physical situation AIP Conf. Proc. 1513 58-61 https://doi.org/10.1063/1.4789651

[20] Mashood K 2014 Development and evaluation of a concept inventory in rotational kinematics *PhD thesis* https://hdl.handle.net/10603/406312

[21] Laws P and Pfister H 1998 Using digital video analysis in introductory mechanics projects *Phys. Teach*. **36** 282-87 https://doi.org/10.1119/1.880068

[22] Williamson J, Torres-Isea R and Kletzing C 2000 Analyzing linear and angular momentum conservation in digital videos of puck collisions *Am. J. Phys* **68** 841-47 https://doi.org/10.1119/1.1302325

[23] Heck A and Uylings P 2005 Yoyo Joy. In: Olivero F and Sutherland R (eds.) *Visions of Mathematics Education: Embedding Technology in Learning* (Proc. ICTMT7, Bristol, UK: University of Bristol) vol 2 237-44

[24] Fäldt Å and Fredlund T 2023 *Phys. Educ.* **58** 025001 https://doi.org/10.1088/1361-6552/aca73a

[25] Hanavan E 1964 A mathematical model of the human body (AMRL TR 64-102) Wright-Patterson Air Force Base, Ohio https://apps.dtic.mil/sti/pdfs/AD0608463.pdf

[26] Robertson G, Caldwell G, Hamill J, Kamen G and Whittlesey 2014 *Research Methods in Biomechanics* (2nd ed.) Human Kinetics https://doi.org/10.5040/9781492595809

[27] Hamill J, Knutzen K and Derrick T 2021 *Biomechanical Basis of Human Movement* (5th ed.) Wolters Kluwer

[28] Hall S 2021 *Basic Biomechanics* (9th ed.) McGraw Hill

[29] Zeni J, Thomas S and Winter D 2023 *Winter's Biomechanics and Motor Control of Human Movement* (5th ed.) Wiley

[30] Zatsiorsky V 2002 *Kinetics of Human Motion* Human Kinetics

[31] Hay G 1993 *The Biomechanics of Sports Techniques* (4th ed.) Prentice Hall

[32] Foss S 1969. A method for obtaining initial estimates of the parameters in exponential curve fitting *Biometrics* **25** 580–4 https://doi.org/10.2307/2528726

[33] Ramsay J and Silverman B 2005 *Functional Data Analysis* (pp 179-81) Springer Verlag https://doi.org/10.1007/978-1-4757-7107-7

[34] Billingsley H 1965 *Diving Illustrated* Ronald Press Company

[35] Frohlich C 1979 Do springboard divers violate angular momentum conservation *Am. J. Phys*. **47** 583-92 https://doi.org/10.1119/1.11759

[36] Edwards M 1986 Zero angular momentum turns *Am. J. Phys*. **54** 846–47 https://doi.org/10.1119/1.14429

[37]Essén H and Nordmark A 2018 A simple model for the falling cat problem *Eur. J. Phys.* **39** 035004 https://doi.org/10.1088/1361-6404/aaac06
[38]Knudson D 2013 *Qualitative Diagnosis of Human Movement: Improving Performance in Sport and Exercise* (3rd ed.) Human Kinetics. https://doi.org/10.5040/9781492596790
[39]Barter J 1957 Estimation of the mass of body segments (*WADC TR 57-260*) Wright-Patterson Air Force Base, Ohio
[40]Clauser C, McConville J and Young J 1969 Weight, volume, and center of mass of segments of the human body (*AMRL TR 69-70*) Wright-Patterson Air Force Base, Ohio https://apps.dtic.mil/sti/tr/pdf/AD0710622.pdf
[41]Woolley, C 1972 Appendix A: Segment masses, centers of mass, local moments of inertia for an anthropometric model of man. In: Conway B A 1972 Development of Skylab experiment T-013 Crew/Vehicle Disturbances (*NASA TN-6584*) NASA Langley Research Center https://ntrs.nasa.gov/api/citations/19720007227/downloads/19720007227.pdf
[42]Hatze H 1980 A mathematical model for the computational determination of parameter values of anthropomorphic segments *J. Biomech*. **13** 833-43 https://doi.org/10.1016/0021-9290(80)90171-2
[43]Nikolova G and Toshev Y 2007 Estimation of male and female body segment parameters of the Bulgarian population using a 16-segment mathematical model. *J. Biomech*. **40** 3700-7
[44]Erdman W 1997 Geometric and inertial data of the trunk in adult males *J. Biomech*. **30** 679-88 https://doi.org/10.1016/S0021-9290(97)00013-4
[45]Huston R 2009 *Principles of Biomechanics* CRC Press
[46]Miller D and Morrison W 1975 Prediction of segmental parameters using the Hanavan human body model *Med.Sci. Sports* **7** 207-12
[47]Project Jupyter https://jupyter.org
[48]Dempster W 1955. Space requirements of the seated operator (WADC TR 55-169) Wright-Patterson Air Force Base, Ohio https://apps.dtic.mil/sti/citations/tr/AD0087892
[49]Whittset C 1963 Some dynamic response characteristics of weightless man (AMRL TR 63-18) Wright-Patterson Air Force Base, Ohio https://apps.dtic.mil/sti/tr/pdf/AD0412451.pdf
[50]Sayyah M 2017 Variability and control in springboard diving *PhD Thesis* University of Loughborough (available at https://hdl.handle.net/2134/33552)
[51]Sotheran A 2019 Real-time analysis and feedback of performance indicators in elite diving *PhD Thesis* Sheffield Hallam University https://doi.org/10.7190/shu-thesis-00397
[52]Tracker Video Analysis and Modeling Tool. https://physlets.org/tracker/
[53]O'Brien R 2002 *Springboard and Platform Diving* (2nd ed.) Human Kinetics
[54]Huber J 2016 *Springboard and Platform Diving* Human Kinetics
[55]Enoka E 2008 *Neuromechanics of Human Movement* (4th ed.) Human Kinetics
[56]Walker C 2017 Functional analysis of stability and variability in multiple forward somersaulting dives from the 3m springboard *PhD thesis* University of Sidney (available at https://hdl.handle.net/2123/17351)
[57]Millar R, Tiberghien A and Le Maréchal, J.-F 2002. Varieties of labwork: A way of profiling labwork tasks In: Psillos D and Niedderer H (eds.) *Teaching and Learning in the Science Laboratory* pp. 9–20 Kluwer Academic Publishers.
[58]Van den Berg E 2009 The PCK of teaching in the laboratory: Turning manipulation of equipment into manipulation of ideas. In: de Jong O and Halim L (eds) *Teachers' Professional Knowledge in Science and Mathematics Education: Views from Malaysia and Abroad* pp 85-110 Faculty of Education, Universiti Kebangsaan Malaysia (available at https://www.iederkindeentalent.nl/wp-content/uploads/2012/06/The-PCK.pdf
[59]Edelson D 1998 Realising authentic science learning through the adaptation of scientific practice. In: Fraser B and Tobin K (eds.) *International Handbook of Science Education* pp. 317-331 Kluwer Academic Publishers